POLITECNICO DI TORINO
Repository ISTITUZIONALE

Remote monitoring of the Comba Citrin landslide using discontinuous GBInSAR campaigns

Original
Remote monitoring of the Comba Citrin landslide using discontinuous GBInSAR campaigns / Barla, M., Antolini, F., Bertolo, D., Thuegaz, P., D'Aria, D., Amoroso, G.. - In: ENGINEERING GEOLOGY. - ISSN 0013-7952. - ELETTRONICO. - (2017). [10.1016/j.enggeo.2017.03.019]

Availability:
This version is available at: 11583/2654423 since: 2017-04-04T16:01:02Z

Publisher:
Elsevier

Published
DOI:10.1016/j.enggeo.2017.03.019

Terms of use:

This article is made available under terms and conditions as specified in the corresponding bibliographic description in the repository

Publisher copyright

(Article begins on next page)

19 June 2026

Contents lists available at ScienceDirect

Engineering Geology

journal homepage: www.elsevier.com

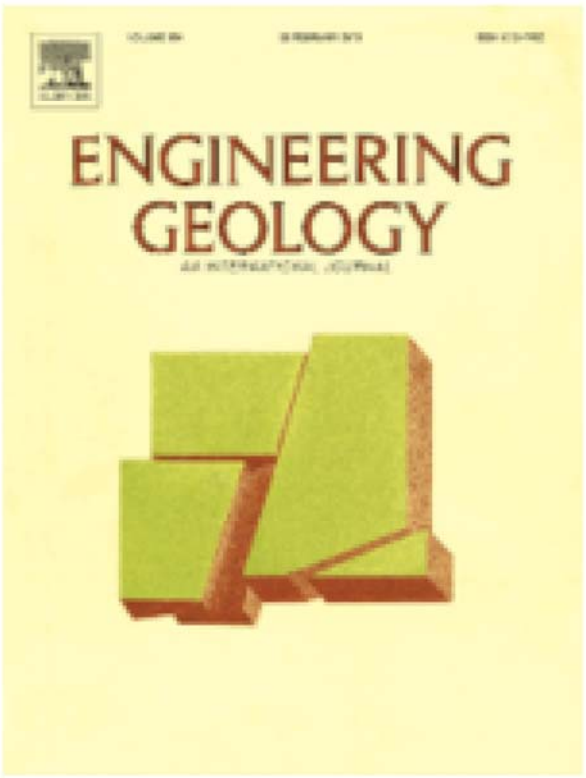

This paper is published on Engineering Geology,
Elsevier B.V., Amsterdam, The Netherlands
DOI: 10.1016/j.enggeo.2017.03.019

The final publication is available at:
http://dx.doi.org/10.1016/j.enggeo.2017.03.019

Remote monitoring of the Comba Citrin landslide using discontinuous GBInSAR campaigns

Marco Barla[1], Francesco Antolini[1*], Davide Bertolo[2], Patrick Thuegaz[2], Davide D'Aria[3], Giovanni Amoroso[3]

[1] Dipartimento di Ingegneria Strutturale, Edile e Geotecnica, Politecnico di Torino, Corso Duca degli Abruzzi 24, 10129 Torino, Italy.

[2] Dipartimento Programmazione, Difesa del Suolo e Risorse Idriche, Regione Autonoma Valle d'Aosta, Loc. Amérique 33, 11020 Quart, Aosta, Italy.

[3] Aresys srl, Via Privata Flumendosa, 16, 20132 Milano, Italy.

* Corresponding author. E-mail: francesco.antolini@polito.it - Tel: +39 011 0904908

Abstract

This paper describes the use of the discontinuous Ground-Based Interferometric Synthetic Aperture Radar technique (GBInSAR) to monitor the displacement of the Comba Citrin landslide in the North Western Italian Alps. Two GBInSAR surveys were carried out respectively during the summer and the fall of 2015 separated by a temporal baseline of 63 days. For each GBInSAR survey, which lasted respectively 166.2 h (6 dd, 22 h, 12') and 238.3 h (9 dd, 22 h, 18'), two sets of 139 and 275 SAR images were acquired. After the selection of a specific stack of Persistent Scatterers, the SAR images of each survey were analyzed separately and in combination with the images of the other survey to detect the possible displacements occurred both in every single survey as well as in the elapsed time between the two different campaigns. The displacement maps showed that two different sectors of the monitored slope were affected by millimetres to centimetres movements during the monitoring period. The results obtained for the Comba Citrin landslide show

that the discontinuous GBInSAR can be reliably adopted to monitor the displacement of landslides moving at an average rate of few centimetres per year.

Keywords: Ground-Based Synthetic Aperture Radar interferometry, Discontinuous monitoring, Landslide, Deformation analysis.

1. Introduction

The Ground-Based Interferometric Synthetic Aperture Radar (GBInSAR) is an active radar-based remote sensing technique, designed in general terms to monitor the displacements of objects (Rudolf et al. 1999, Tarchi et al. 2003). In the last fifteen years, the GBInSAR has proven to be a powerful tool for monitoring displacements and deformation affecting natural and engineered slopes, glaciers and volcanic flanks (e.g. Barla et al. 2010, Casagli et al. 2010, Intrieri et al. 2013, Farina et al. 2013, Strozzi et al. 2012) as well as for monitoring structural deformation (e.g. Barla & Antolini 2015a, Alba et al. 2008, Tapete et al. 2013). A comprehensive review of the state of the art of the ground-based SAR interferometry technique and its main application can be found in Atzeni et al. (2015) and in Monserrat et al. (2014).

Two different acquisition modes, namely continuous GBInSAR and discontinuous GBInSAR, can be applied to monitor the displacements of natural, engineered slopes and man-made objects (Monserrat et al. 2014).

In continuous GBInSAR monitoring, the radar sensor is generally installed in a stable position, i.e. an area not affected by deformation, and it acquires data at regular intervals during a unique survey which can last up to several months or years. This approach is particularly suitable to monitor landslides belonging to velocity classes 3 and 4 up to 2.1 m/day (Fig. 1) and for mining applications (Barla & Antolini, 2015b). In the same Fig. 1 the time to reach the ambiguous displacement of $\lambda/4$

for a radar device with wavelengths of 17.4 mm (Ku band), similar to the instrument used in this work, is also indicated. Due to the fact that the minimum scan time to acquire two consecutive SAR images varies from about 3 to 9 min. (depending on the radar model and on the scanned range), the maximum unambiguous velocity which can be monitored lies in the range 0.7 – 2.1 m/day. If the slope is moving at higher velocity, the intrinsic phase ambiguity of the interferometric technique hinders the correct measurement of the real displacement.

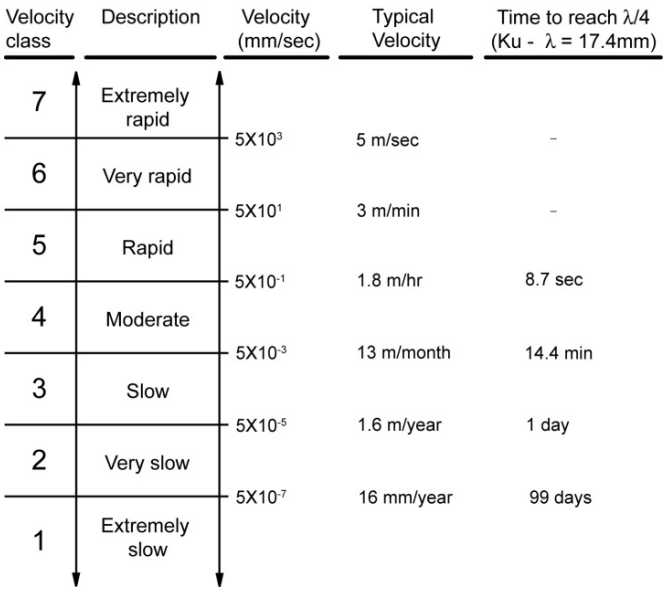

Fig. 1 – Landslides velocity scale by Cruden & Varnes (1996) compared to the time to reach ambiguous displacement for a radar device working at Ku band (λ = 17.4 mm) (Antolini, 2014).

When very slow and/or extremely slow slope displacements are expected, i.e., the velocity rate is comprised between few mm per years to few cm per years, a more efficient monitoring approach is the discontinuous GBInSAR monitoring. Very slow and extremely slow moving landslides are widespread in the Alpine region and, despite the low seasonal velocity, need to be constantly monitored to early detect the possible acceleration phases. For these applications, in addition to space-borne InSAR (Wasowski and Bovenga, 2014a, 2014b), the discontinuous GBInSAR monitoring may be a cost-effective alternative to continuous GBInSAR and to point-wise in situ

monitoring systems. Few works dealing with discontinuous GBInSAR applications currently exist, e.g. Corsini et al. (2011), Crosetto et al. (2014), Noferini et al. (2005b, 2008) and Luzi et al. (2010).

The correct discontinuous GBInSAR displacement estimation requires solving two main issues related to the processing of SAR imagery:

- the geometric baseline, i.e. the topographic phase component introduced by the inaccurate re-positioning of the system;
- the temporal decorrelation, i.e. the loss of coherence between different surveys separated by large time span (i.e. weeks or months).

Both the aforementioned issues, if not rigorously treated in the SAR images processing chain, represent a severe limitation for a reliable discontinuous measurement of slope displacement.

Generally if a concrete base and a precise mechanical positioning system is used (as in this work), the geometric baseline is zero. This avoids the need of any further processing step devoted to estimate and remove the topographic component in the interferograms.

The processing limits caused by temporal decorrelation were overcome by using Permanent Scatterers Interferometry (Ferretti et al. 2001) on the full temporal data stack of SAR images acquired in the different surveys. The approach is similar to the small baseline technique adopted in the processing of satellite-borne imagery (Berardino et al. 2002). To correctly solve the phase ambiguities in the interferograms, Noferini et al. (2008) integrated the approximate prior knowledge of the monitored slope deformation velocities in the phase unwrapping algorithm. Another indirect approach to solve the ambiguities related to radar measurements was proposed by Wujanz et al. (2013) through an integration between real aperture radar (RAR) and Terrestrial Laser Scanning (TLS) on an experimental site.

In the present work, the SAR images acquired by a radar interferometer working at Ku band (central frequency equal to 17.2 GHz) are used to estimate the displacement between two surveys, separated

by a temporal baseline of 63 days, using specific software. In particular, all possible images pairs of two different campaigns are considered, and for each pair, the complex coherence is evaluated. Using the complex coherence, it is possible to sort the best interferograms to be used to perform the displacement estimation. The selected interferograms are unwrapped, averaged and cleaned from the atmospheric phase screen (APS) and the resulting unwrapped phase is then converted to line-of-sight slope displacement. The objective of this work is therefore to test the applicability of the discontinuous GBInSAR technique and this specific processing method to the Comba Citrin landslide, located in the NW Italian Alps. Finally, the validity of the obtained results is discussed in the view of a new interpretation of the landslide kinematic.

2. GBInSAR monitoring of the Comba Citrin landslide

The Comba Citrin landslide is located in the Valle d'Aosta Region (NW Italian Alps), very close to Italy-Switzerland border and about 20 km north of Aosta city. The landslide lies on the NW face of the Tete du Bois de Quart ridge. This mountainous ridge extends in NW-SE direction from the top of Flassin Mount towards the valley of the river Artanavaz and the Saint Rhémy en Bosses village (Fig. 2a).

2.1 Geologic and geomorphologic setting

The landslide affects the albite- and chlorite-bearing paragneiss and the carbonate micaschists belonging to the Flassin Unit of Palaeozoic age. The Flassin Unit is located close to the contact with the micaceous metarenites and the graphitic-phyllitic schists of Carboniferous age of the Zone Houllière (Fig. 2b). These two units constitute respectively the crystalline basement and the sedimentary cover of the Brianzonese Zone. The contact between the two units corresponds to the valley of the Citrin stream.

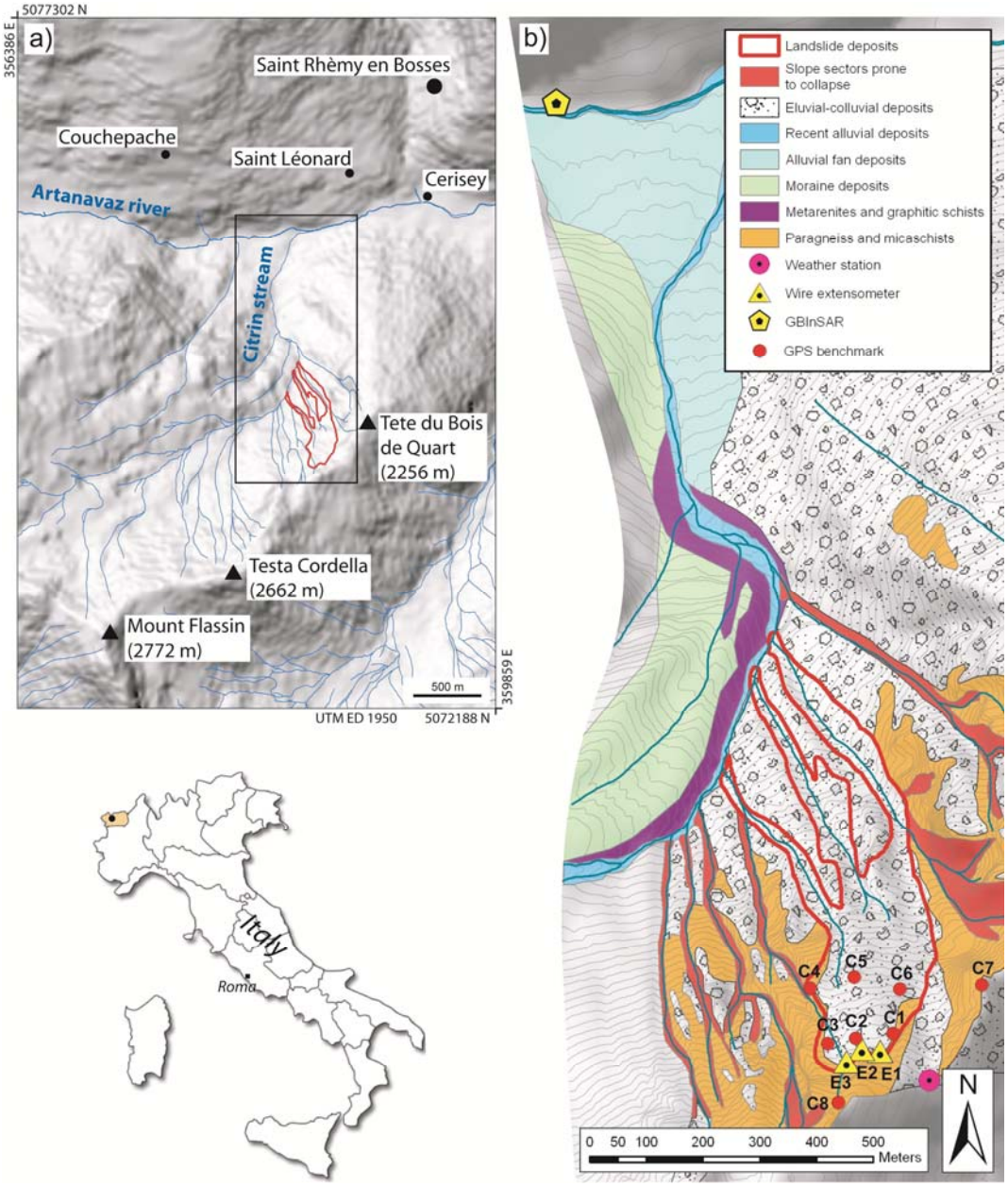

Fig. 2 – a) The location of Comba Citrin landslide; b) Geological sketch of the studied area.

The Comba Citrin slope instability is the reactivation of a quiescent landslide which took place during an intense rainfall event in October 2000. The event caused also an extensive flooding in the Valle d'Aosta Region (Ratto et al. 2003). The instability can be classified on the whole as a complex-

composite rock and debris slide-debris flow. The slide moves on a compound surface (i.e. rotational/planar) and affects both the bedrock and the debris cover on the slope (Fig. 2b). The multi-temporal photo interpretation analysis along with the geophysical surveys carried out in the past years (Hydrodata, 2005) indicated that the landslide's rupture surface is located at depth variable from 10 to 30 m from the topographic surface and it is progressively enlarging, especially along the sides. The landslide's crown zone is characterized by falls and topples affecting portions of highly fractured rock mass. The more superficial layer of collapsed material evolves also as debris flow along three main gullies. These incisions converge down slope in the Citrin stream, tributary of the Artanavaz river. Close to the landslide area there are further incisions where endemic collapses (i.e. rock falls and topples) take place resulting in the accumulation of debris along the slopes.

The volume of the material involved in the reactivation of October 2000 was estimated to be equal to 400,000 m^3 (Hydrodata, 2005). The potential risk caused by the landslide lies in generating debris flows which, in the worst scenario, could cause a barrier lake on the Citrin stream. The potential collapse of the landslide's dam could in turn generate a debris flow/flood threatening the villages of Saint Oyen and Étroubles. For this worst case scenario a total mobilizable material volume equal to 1,500,000 m^3 was estimated (Hydrodata, 2005).

At present the landslide is monitored by three extensometric devices, periodic D-GPS measurements on 8 targets and a weather station. The extensometric devices, namely E1, E2 and E3, are installed across the main tension crack in the landslide crown area (Fig. 2b). Each extensometer is made up by a potentiometric cable extension position transducer connected to a further stainless steel wire (diameter of 2.5 mm) fixed to a stake hammered on the ground on one end and a pulley with a counterweight which is free to roll on the other end (Fig. 3). The length variations of the 2.5 mm stainless steel wire caused by the crack opening/closing triggers a rotation of the pulley and a consequent length variation of the cables of the potentiometric transducers.

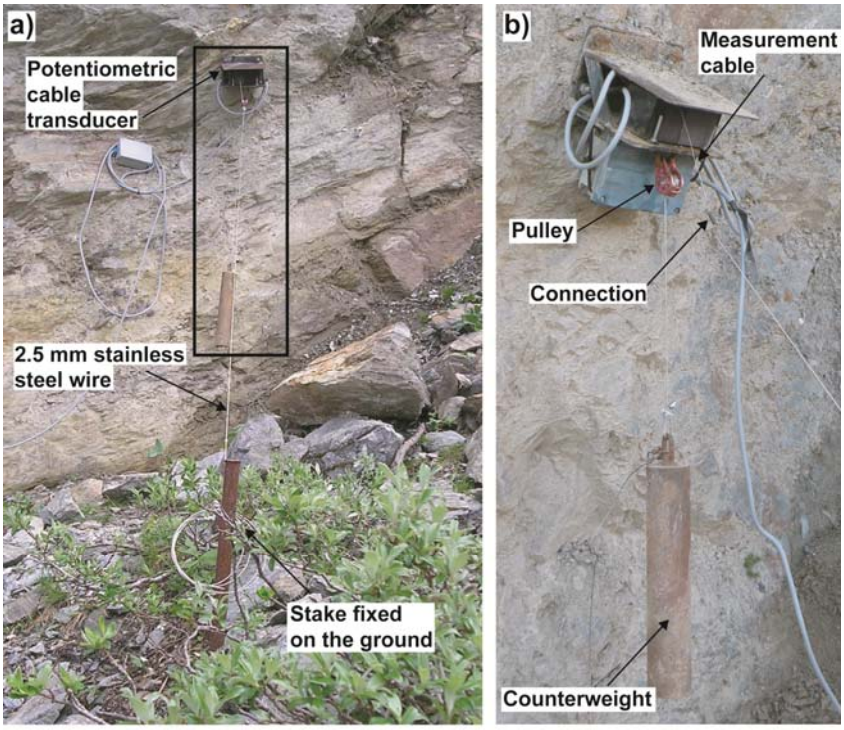

Fig. 3 – a) E2 extensometric device setup; b) Detailed view of the arrangement of the measurement system.

The monitoring system is directly managed by the Geological Department of the Regione Autonoma Valle d'Aosta. In addition, D-GPS measurements on 8 targets distributed on the landslide (Fig. 2b) were carried out yearly. However, such monitoring system is not sufficient to monitor the behaviour of the slope. The information given by the D-GPS is in fact only point-wise whereas extensometers experienced frequent wreckages caused by snowfalls during winter and their overall reliability in the current setup is considered low.

2.2 GBInSAR surveys

Two GBInSAR monitoring surveys were carried out, the first one from July 29th to August 5th 2015 and the second one from October 7th to October 16th 2015 (Table 1). The radar instrument was

installed on a stable concrete wall along a local road in the municipality of Saint Rhémy en Bosses. From this position the Comba Citrin landslide lies between 1100 m and 2200 m away from the sensor (Fig. 4) and a good coverage of the area to be monitored is ensured.

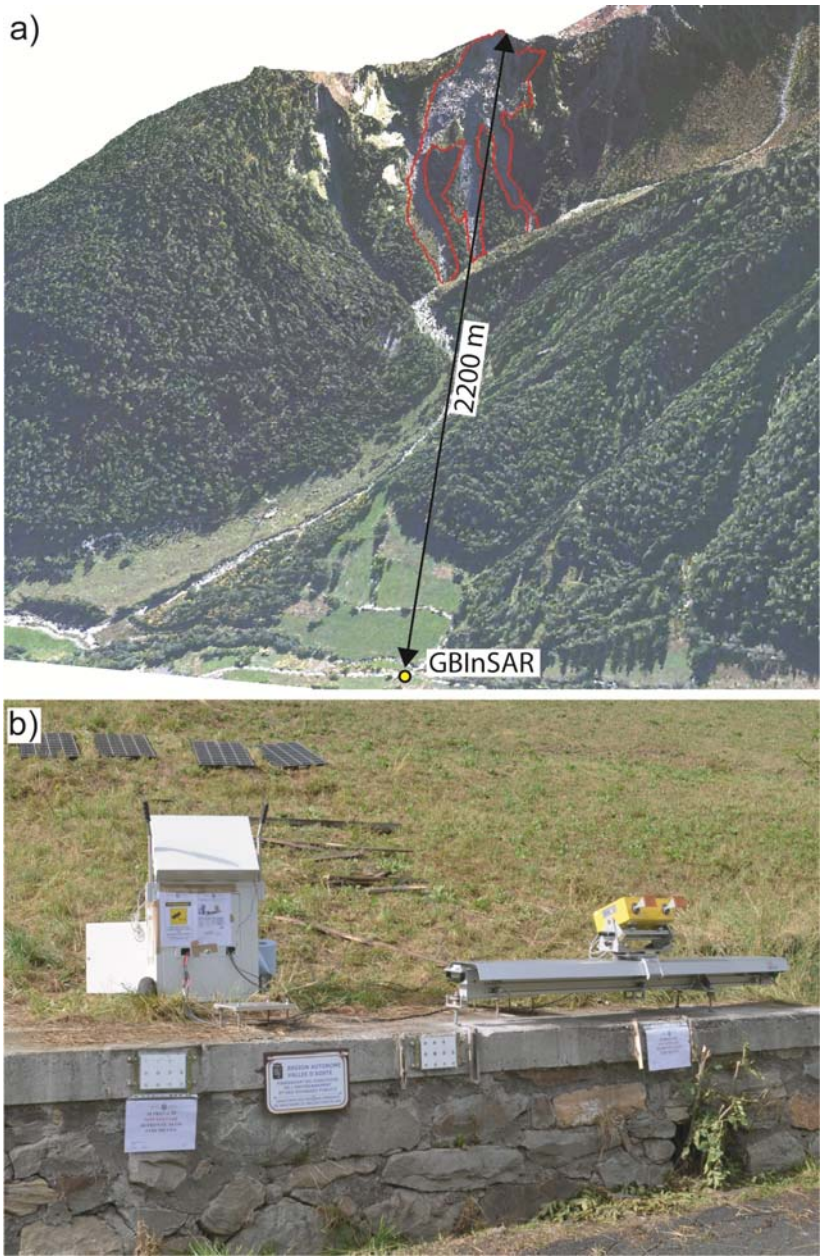

Fig. 4 – a) View of the radar location with respect to the Citrin landslide and b) GBInSAR system set-up.

The radar anchoring system adopted has been developed to allow an easy and exact repositioning of the instrument and to avoid the introduction of geometric baseline in subsequent measurement campaigns. Given the absence of a network power supply, the system was connected to four photovoltaic modules coupled with batteries (Fig. 4b).

A total of 139 and 275 SAR images were acquired respectively during the first (July-August 2015) and the second monitoring survey (October 2015). The average SAR images sampling interval for the two campaigns was respectively 70' and 50' while a single SAR image acquisition lasts about 9 min.. The longer sampling interval during the first survey was caused by a few radar system interruptions: during cloudy day the photovoltaic modules were in fact not able to provide the power supply.

The main characteristic of the two different SAR surveys are summarized in Table 1 while the main instrumental parameters adopted are summarized in Table 2.

Table 1 – Summary of the main characteristics of the Comba Citrin GBInSAR monitoring campaigns.

	Start date	End date	Duration	SAR images acquired	Average SAR images sampling
First SAR campaign	29/07/2015, 16:31	05/08/2015, 14:43	6 dd, 22 h, 12'	139	70'
Second SAR campaign	07/10/2015, 12:24	16/10/2015, 10:42	9 dd, 22 h, 18'	275	50'

Table 2 – Instrumental parameters adopted for the GBInSAR monitoring campaigns.

Central frequency	17.2 GHz
Bandwidth	300 MHz
Synthetic Aperture	2 m
Polarization	VV
Linear scansion points	401
Antenna	Horn 20 dB
Antenna aperture (-3 dB beamwidth - elevation)	15°
Antenna aperture (-3 dB beamwidth – azimuth)	17°
Target distance	1200 – 2200 m

To georeference the SAR images, the coordinates of the radar installation point were measured by means of a geodetic GPS. Table 3 shows the coordinates of the starting, central and ending points of the synthetic aperture, along with the Line Of Sight (LOS) pointing angle and the inclination of the system.

Table 3 – Radar Installation coordinates, LOS direction and inclination.

	Lat WGS84	**Long WGS84**
Scan starting point	45°49'05.19183"N	7°10'17.88995"E
Scan ending point	45°49'05.16437"N	7°10'17.77724"E
Scan central point	45°49'05.17811"N	7°10'17.83404"E
LOS pointing angle (clockwise from N)	173°	
LOS inclination (above the horizontal plane)	+20°	

2.3 GBInSAR images processing

To measure the displacement of the Comba Citrin landslide, both continuous and discontinuous SAR images processing schemes were used. By means of a continuous processing scheme, the images stacks of each survey have been processed separately. By using a discontinuous processing, all the acquired images of the two surveys were used in combination to identify the best interferograms and to detect the overall displacements of the slope.

This work flow allowed measuring the possible displacements occurring within each survey as well as the very slow seasonal movement of the landslide. For the two different processing schemes different software were used, respectively the software GRAPeS (Aresys, 2014) and the software Repeat Pass (Aresys, 2015) both based on Persistent Scatterers (PS) interferometry. The detailed description of the continuous processing scheme and the software GRAPeS is out of the scope of this paper and can be found in Antolini (2014), Barla et al. (2010) and Mariotti et al. (2012).

When dealing with long observational times, lots of pixels in the SAR images can easily be affected by temporal decorrelation and/or phase noise. The selection of a set of sufficiently coherent pixels to ensure a reliable interferometric analysis was carried out, both in the continuous and

discontinuous analysis, by exploiting the PS technique (Noferini et al., 2005a). The PS were identified by calculating the amplitude dispersion index (ADI) using all the SAR power images available for each campaign. For each pixel (i,j) in the SAR images the ADI is calculated as:

$$\boldsymbol{ADI(i,j) = \frac{Std[A_1(i,j), \dots, \dots, A_n(i,j)]}{MA(i,j)}} \quad (1)$$

where A_1, A_n represent the amplitude values of the pixel i,j in the n-th SAR image. Due to its statistical meaning, at least 30 different SAR images are needed to calculate the ADI. Pixels exhibiting an ADI lower than 0.25 were chosen as PS. No multi-looking and no oversampling of SAR images were applied before the PS selection. The PSs are almost all distributed on rocky and debris areas and where scarce vegetation is present. Some PSs have been however identified also in slope sectors with trees. This means that in the same resolution cells further stable scatterers targets (i.e. rock blocks) are present, satisfying the required ADI threshold.

Three different PS stacks were respectively obtained: one for the first survey (July-August campaign), another for the second survey (October campaign) and the last for the discontinuous survey. The latter PS stack obtained by exploiting all SAR images was used to calculate the different interferograms between the first and the second survey.

In addition for each interferogram the complex coherence γ value was calculated according to the following equation:

$$\boldsymbol{\gamma = \frac{\sum_{n=1}^{N_{PS}} M \cdot S^*}{\sqrt{\sum_{n=1}^{N_{PS}} |M^2| \cdot \sum_{n=1}^{N_{PS}} |S^2|}}} \quad (2)$$

where M and S are respectively the master and the slave image and $*$ is the complex operator. This value is in the range [0,1] and describes the phase alignment between master and slave images for each PS, less than a phase constant. A small value of γ means a very high decorrelation, while γ equal to 1 means that the master and slave images are well aligned in phase.

Fig. 5a shows the PS coherence matrix obtained for all the image pairs which have been processed. The trend of coherence, differently to what expected, seems not correlated with day/night alternations. The interferogram obtained with the images acquired from 9th to 10th October are characterized by the highest coherence values. On the contrary specific time spans characterized by lower coherence are evident, in particular from 1st to 2nd August 2015 (first survey), during 11th October 2015 and from 14th to 16th October 2015 (second survey). These low coherence intervals are mainly related to rainfalls/snowfalls occurrences, causing important changes of the soil moisture content of the target area.

In the case of the discontinuous processing, the best 40 interferograms characterized by the highest coherence values were selected from the obtained coherence matrix and used to retrieve the displacement occurred between the two surveys. For instance in the Fig. 5b the best interferogram obtained by combining the master image acquired on 2nd August 2015 at 21:28 with the slave one acquired on 8th August 2015 at 22:31 and characterized by the maximum value of coherence (red square in Fig. 5a) is shown.

After the selection, the spatial phase unwrapping of each interferogram was performed, and then the Atmospheric Phase Screen (APS) was modelled by a polynomial function of specific order estimated with a least square fitting method on stable areas (i.e. areas not affected by movements). The estimated APS model was successively removed from the same unwrapped interferogram. The APS model therefore does not affect at all, or affect at a very low level, the points in the images characterized by real movements. This results from the assumption that APS has generally a low pass spatial behaviour on the whole interferogram. The APS estimation and removal was performed after the interferograms selection to reduce the computational cost in the processing chain. Each unwrapped interferogram was then an estimation of the displacement occurred between the

corresponding master & slave pair and finally all the 40 estimations were averaged to further reduce noise.

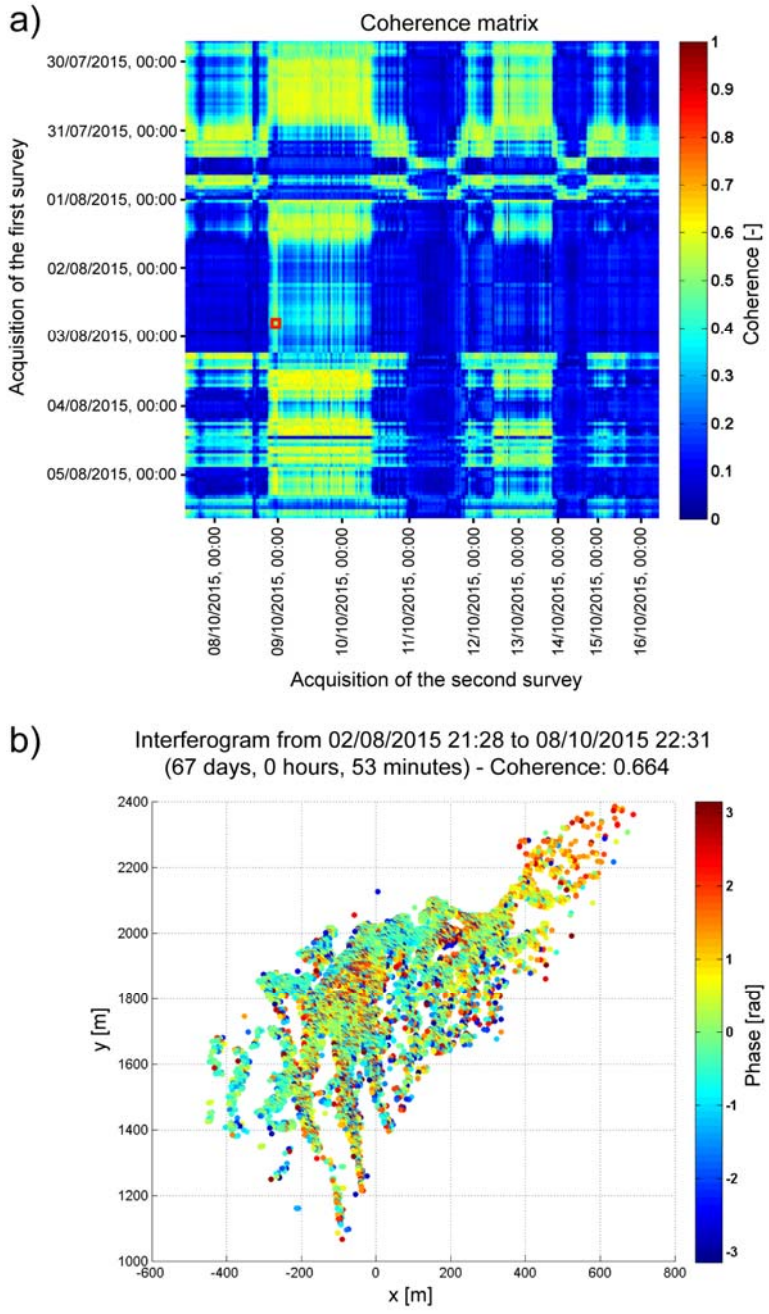

Fig. 5 – a) Coherence matrix between each pairs of SAR images acquired during the two weekly GBInSAR surveys; b) Highest coherence interferogram (0.644) obtained; the phase of the interferogram is wrapped in the range $\pm \pi$.

Fig. 6 shows the averaged unwrapped interferogram after the APS compensation. The map is helpful to detect areas not affected by movements, i.e. the slope's sectors surrounding the main landslide body where the phase values are spatially correlated and close to zero. The ambiguity related to the constant absolute phase is automatically resolved by the APS removal since the selected stable areas must have an absolute phase close to zero which derives from the assumption of the absence of displacement.

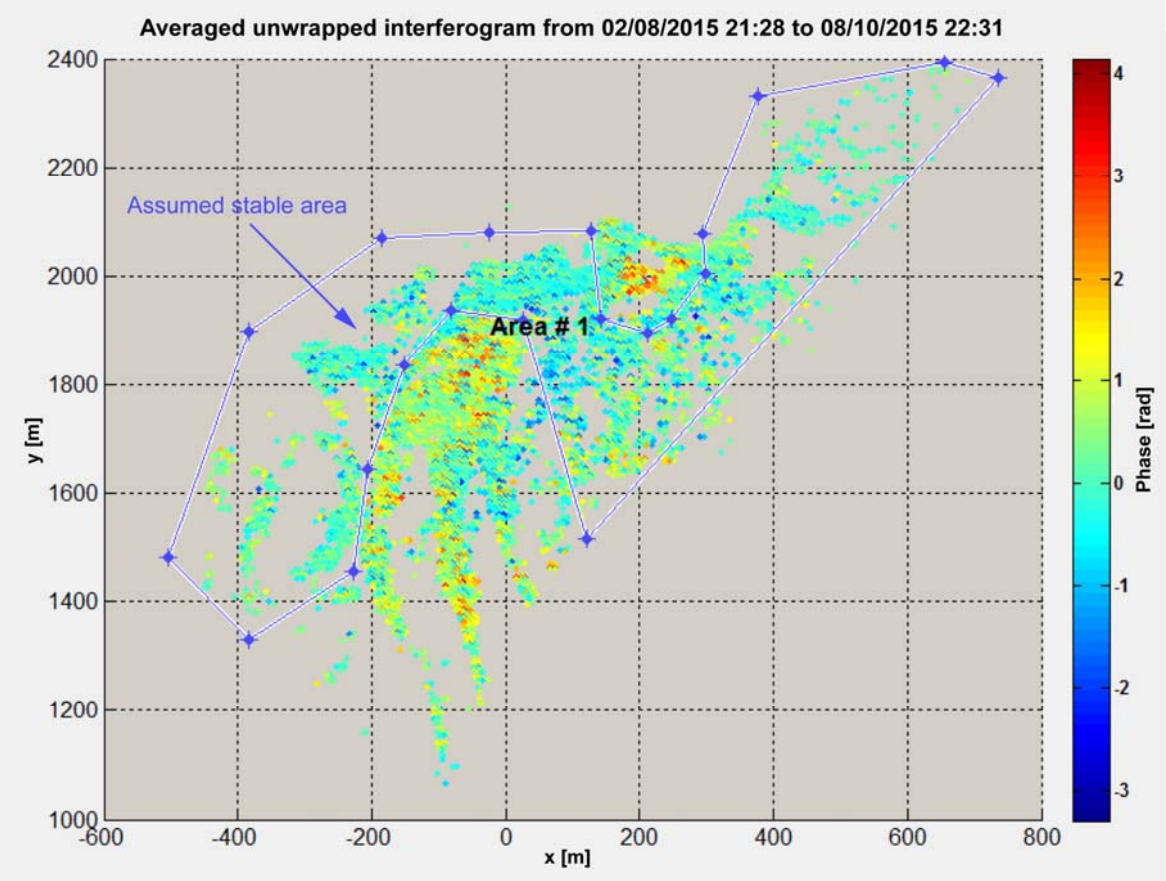

Fig. 6 – Averaged unwrapped and APS compensated interferogram. The highlighted area represents the assumed stable area adopted for APS correction.

2.4 Results of the GBInSAR monitoring

In this chapter the results of the continuous as well as the discontinuous processing will be shown in details. At first the power SAR images were analyzed to allow for the identification of the different features on the monitored scenario. The interpretation of the SAR scene is generally not straightforward since the geometry of a SAR image cannot be directly compared to the geometry of optical imagery due to the different projections used.

By comparing the selected PS power map with an optical image taken from the same GBInSAR acquisition point, the common areas were matched. The whole monitored scenario was therefore subdivided into 5 main sectors (Fig. 7):

- Sector A, corresponding to the main landslide body;
- Sector B, corresponding to the landslide's crown zone and the upper rock faces;
- Sector C, corresponding to the gullies located downstream of the zone A where the collapsed material is further mobilized as debris flows;
- Sector D, corresponding to the slope sectors located to the west of the landslide;
- Sector E, corresponding to the slope sectors located to the east of the landslide.

For the two continuous surveys the final results of the processing are expressed in terms of geocoded LOS displacement and velocity maps. These maps represent pixel by pixel the changes in the monitored scenario which took place from the beginning to the end of each survey. The displacement is always measured along the line of sight of the radar (one-dimensional measurement). Negative displacement indicates a decrease of the sensor to target distance.

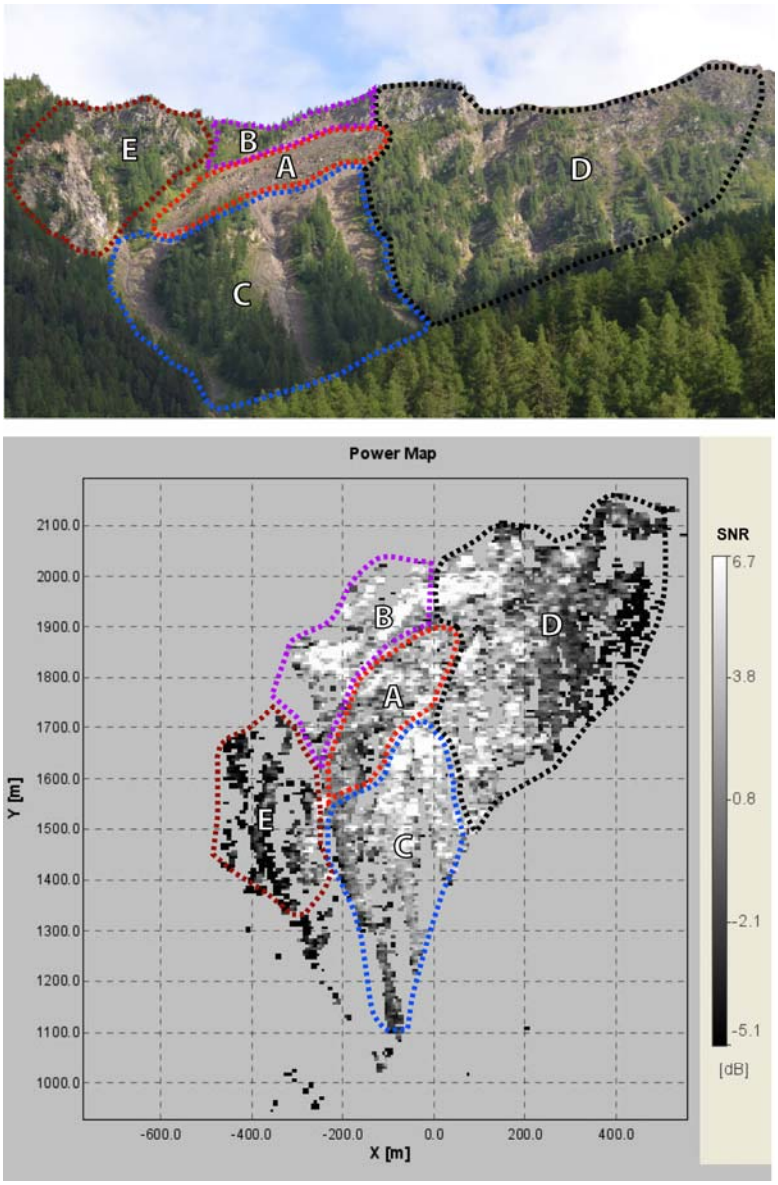

Fig. 7 – Comparison between optical image and SAR power map of the selected PS (October SAR survey) showing the whole monitored scenario with the different slope sectors (A, B, C, D, E) described in the text. The optical image was acquired from the radar installation point.

The results of the first (July-August 2015) and the second survey (October 2015) are respectively shown in Fig. 8a and Fig. 8b. The pixels in the maps are equal to 6x6 m.

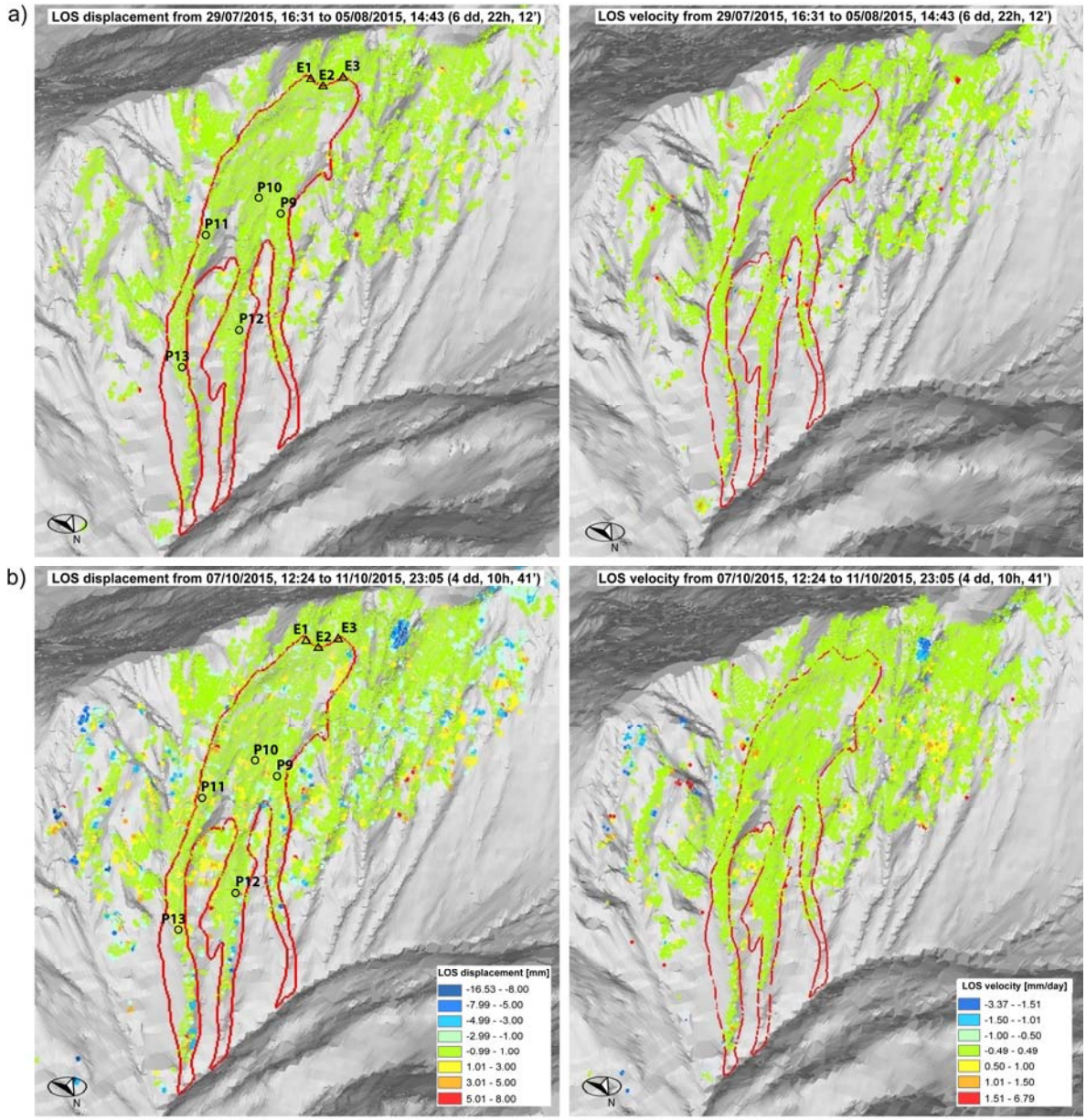

Fig. 8 – Cumulated LOS displacement and LOS velocity maps of the first (a) and the second (b) GBInSAR surveys projected over a Digital Elevation Model of the area. The landslide boundaries are shown by the continuous red line. The black triangles show the position of the extensometric devices (E1, E2 and E3) while the black circles indicate the selected time series points (P9, P10, P11, P12 amd P13) shown in Fig. 9. (For interpretation of the references to colour in this figure legend, the reader is referred to the web version of this article.)

The LOS displacement map of the first monitoring survey (Fig. 8a) shows a substantial absence of significant movements, highlighted by green pixels in the maps, over the landslide body as well as in

the surrounding areas. Some isolated pixels showing spatially discontinuous movements, generally correspond to areas with partial vegetation coverage and, despite having been selected as PS, are characterized by a low interferometric quality. The analysis of time-series (Fig. 9a) shows that the displacement of these points during the survey was in the range ±0.25 mm, which is roughly equal to the accuracy of the measurements.

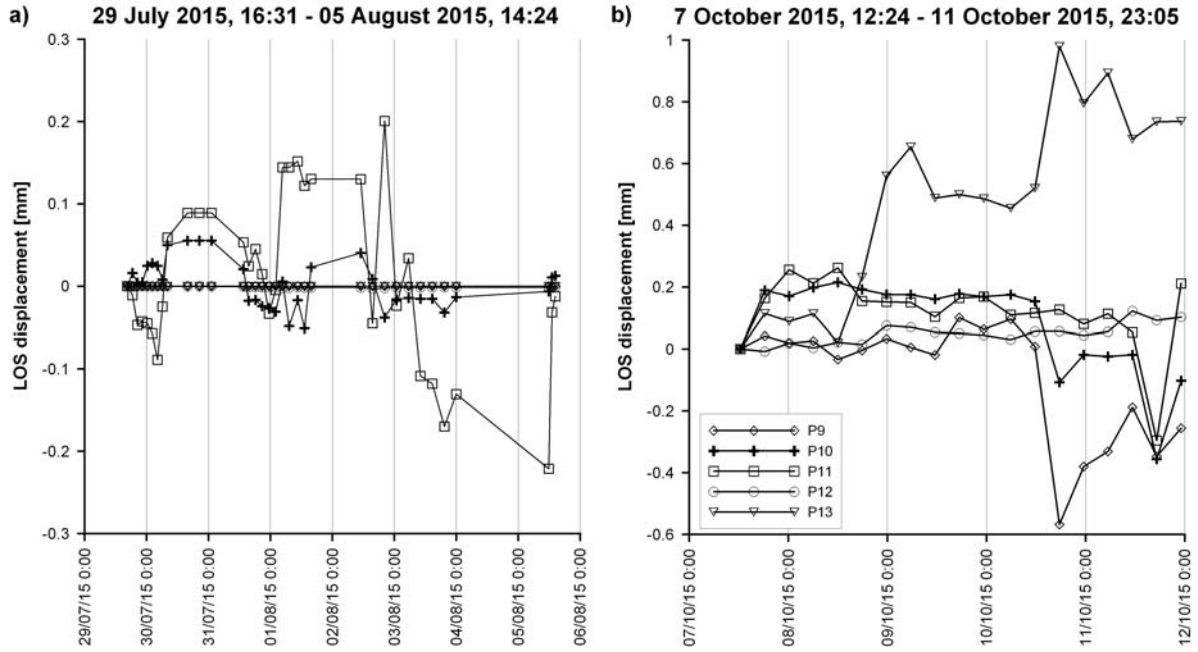

Fig. 9 – Time series of selected points on the landslide during the first (a) and the second (b) GBInSAR survey. The position of each point is shown in Fig. 8.

The LOS displacement pattern retrieved from the second survey shows instead a higher complexity. In particular, given the overall absence of movement on sectors A, B, C and D, the displacement map highlights the presence of an area in E sector, with approximate size of 40 x 50 m, affected by negative displacements compatible with a progressive sliding downhill (Fig. 10a). The time series data shown both in Fig. 9 and Fig. 10c were sub-sampled to reduce the computational effort of the software during the processing.

This area is actually outside the Citrin landslide body and it was not included in any landslide's inventory. The deformation affects a portion of highly fractured rock mass and a portion of debris lying at the base of very steep rock faces (Fig. 10b).

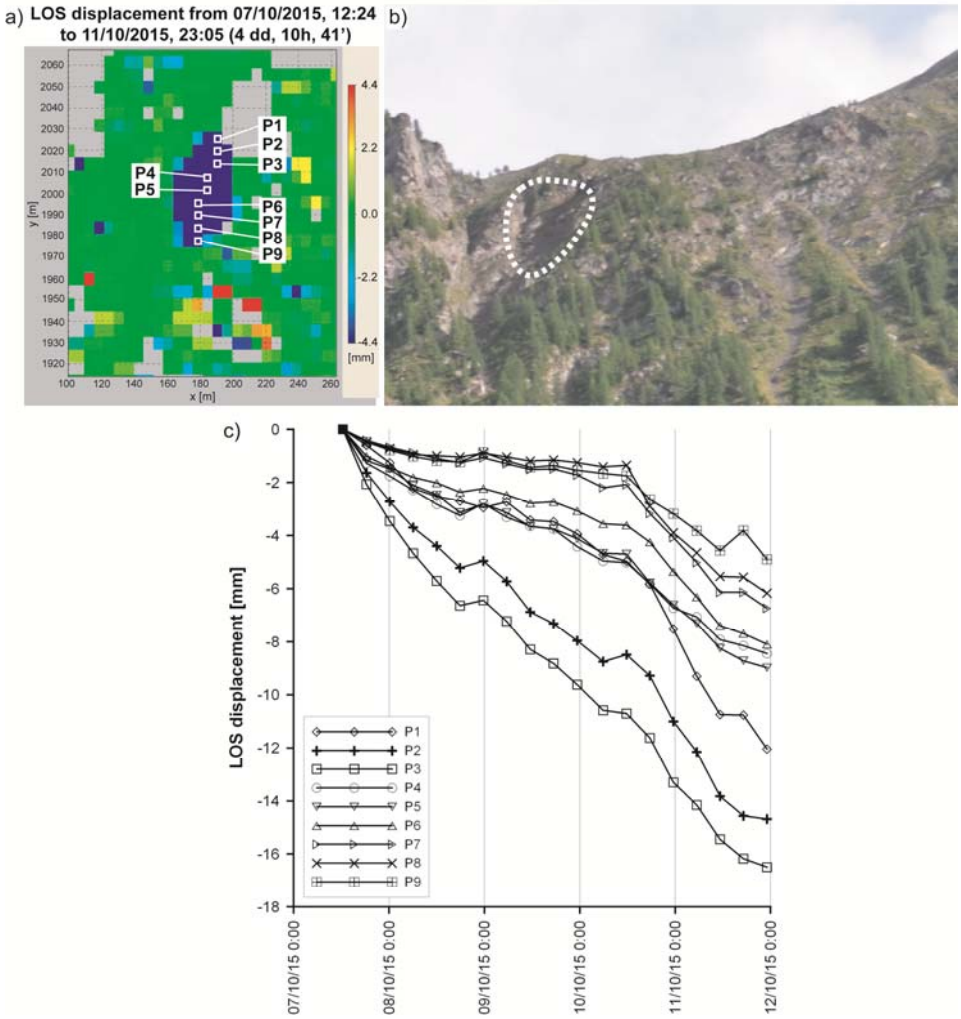

Fig. 10 – a) Detail of the displacement map obtained from the second GBInSAR survey (October 2015); b) optical image showing the area affected by major deformations; c) time series of nine points extracted from the area affected by major deformations.

The analysis of the sequential daily cumulated LOS displacement maps reveals that the same area has been widened during the monitoring survey, progressively extending in space as shown in Fig. 11. The sequential LOS displacement maps shows that the displacement originated at the apex of a

system of deep gully incisions and then progressively extended down slope up to a total length of about 50 m.

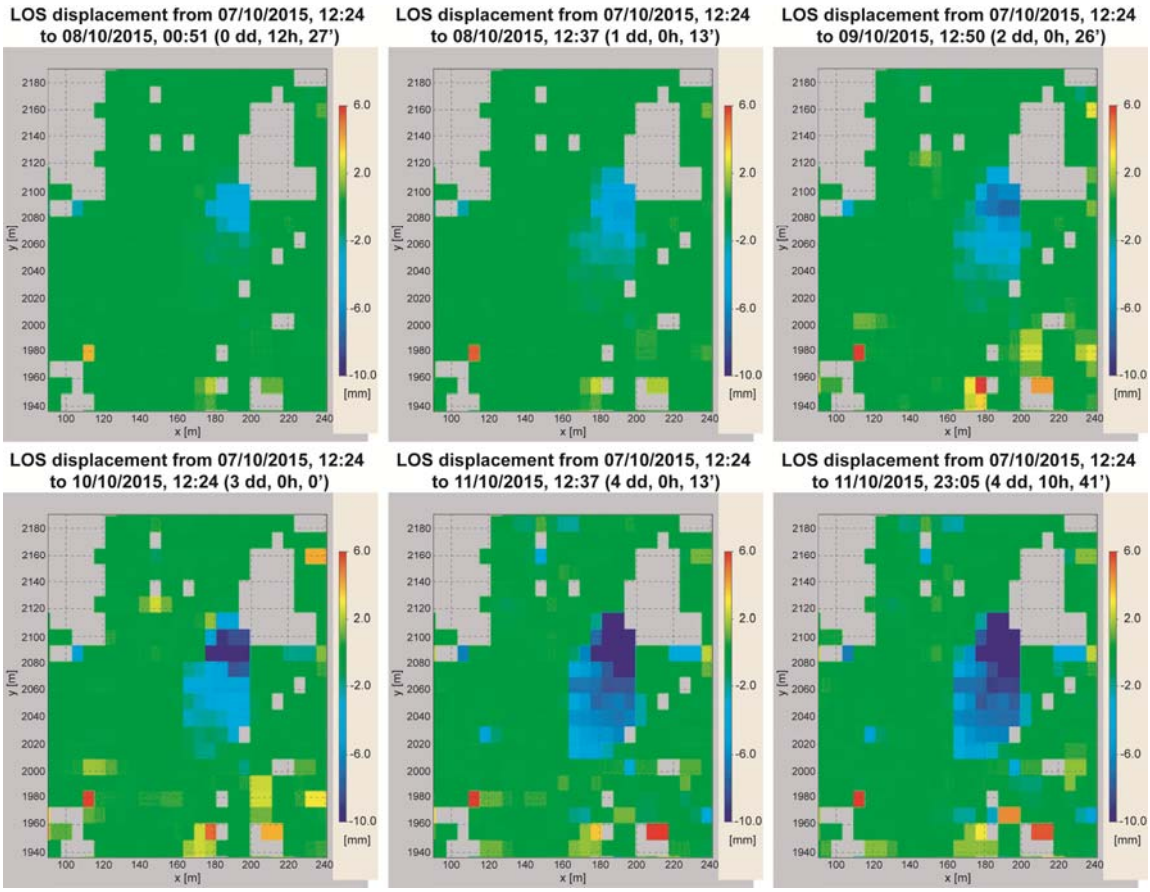

Fig. 11 – Sequential LOS displacement maps obtained from the second GBInSAR survey (October 2015) showing the spatial evolution of the sector affected by major deformations.

The maximum LOS displacement reaches -16.5 mm, whereas for the majority of the points lies between -4 and -7 mm (Fig. 10c). The maximum LOS displacement rate recorded was equal to 3.5 mm/day. By assuming a main component of displacement nearly parallel to the average slope's dip and dip direction (this assumption appears reasonable in the view of the recognised types of instability), the projected angles between the radar LOS and the direction of displacement vectors of the points P1-P9 in the range-cross range plane are in general smaller than 5°. Therefore, even if this

sector is located laterally to the main landslide body, the sensitivity of the radar LOS measurement to real displacement can be considered very high.

Similarly to the first survey, the A, B, C and D sectors resulted stable.

The LOS displacement map obtained by the discontinuous GBInSAR, is shown in Fig. 12. The displacement map shows the presence of two different areas affected by movements.

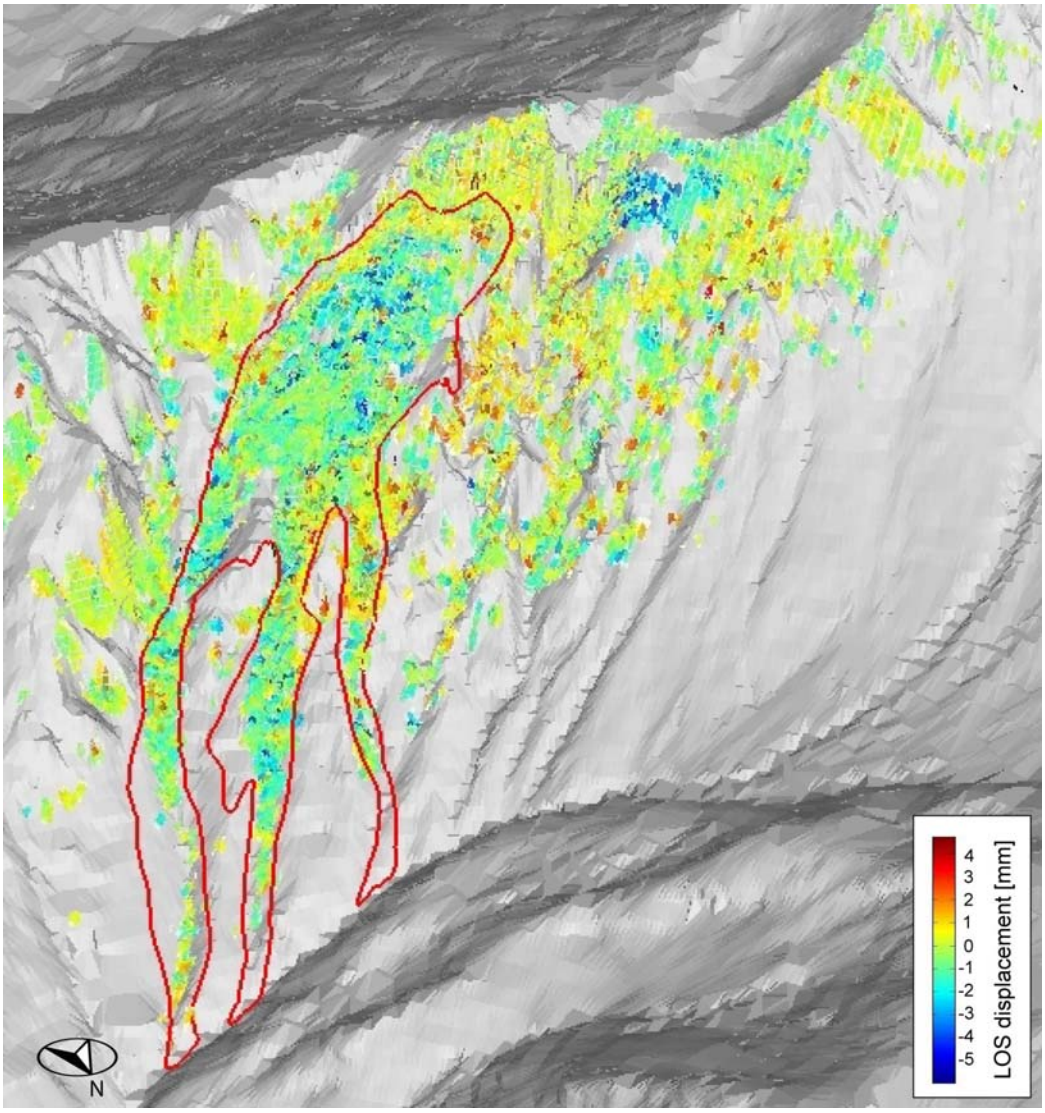

Fig. 12 – Results of the discontinuous GBInSAR monitoring: LOS displacement map from August 2nd 2015 to October 8th 2015 projected over a Digital Elevation Model (DEM) of the area. The Comba Citrin landslide boundaries are shown by the continuous red line. (For interpretation of the references to colour in this figure legend, the reader is referred to the web version of this article.)

The easternmost moving area substantially matches the Comba Citrin landslide body and the gullies located downstream (A and C sectors). Larger LOS displacements, between -3 mm and -5 mm were measured in the central and the upper portions of the landslide body. Proceeding towards the base of sector A, as well as in sector C, a progressive reduction of the displacement, particularly in the western portion of the landslide body, is evident. Along the detrital gullies of sector C (Fig. 7) the measured LOS displacements are generally comprised between -1 and -2.5 mm, even though they are not homogeneous. Only few isolated pixels showed maximum displacements up to -4 mm. The further area affected by movements is located to the west of the main landslide body and retrace the moving area in the sector D which has been identified during the October survey (Fig. 8b). In this area from August 2nd 2015 to October 11th 2015 the LOS movements exceeded -6 mm. The spatial distribution of displacement shows a slightly larger affected area than the moving sector identified during the second survey thus confirming that this unstable sector has progressively enlarged.

During the short time span of the continuous radar surveys, the whole monitored slope sector appeared as not affected by any movements, except from the moving area in sector D which has been identified during the October survey. A larger time span of monitoring was necessary to measure the displacements of the landslide body through the discontinuous SAR images analysis. The average LOS velocity of the Comba Citrin landslide body retrieved through the discontinuous survey and comprised roughly between -1.0 and -2.5 mm/month appears to be in good agreement with the displacement velocities between 5 and 20 mm/year measured during 2015 on the six GPS benchmarks C1-C6 shown in Fig. 2 (Regione Autonoma Valle d'Aosta, personal communication).

In the view of this, the reliability of the discontinuous GBInSAR analysis can be considered high inside the Comba Citrin landslide boundaries which are characterized by very slow displacement and slow spatial gradient, i.e. movement which varies gently in space without abrupt changes. Faster displacements, as those of the area located to the west of the main landslide body, could imply a

shift of phase cycles between the two discontinuous surveys that could not be correctly retrieved if no a priori information on velocity is available (Noferini et al. 2008). Therefore the measured deformation of the area located to the west of the main landslide body from August to October 2015 suggests two possible alternative interpretations for the onset of displacement:

- displacement could have started almost at the same time of the beginning of the second campaign or very close to it;
- displacement could have started in an undefined time between the two surveys and the ambiguous displacement in the area has been exceeded.

Since the displacement map in Fig. 12 does not show a critical loss of coherence of the moving areas, this suggests that the deformation has started very close to the beginning of the second survey, i.e. on the 7th October 2015. In particular by the end date of the discontinuous analysis, i.e., 8th October 2015 at 22:31, the maximum LOS displacement of the sector was comprised between -2 and -6 mm (Fig. 12) while the continuous survey of October has retrieved a maximum displacement of -16.5 mm up to 11th October 2015 at 23:05. Therefore the presence of phase jumps, resulting in an underestimation of the total displacement in this faster moving sector cannot be completely excluded.

By integrating the displacement information retrieved within the GBInSAR data for this area is possible to conclude that from August to October 2015 this unstable sector underwent a most likely acceleration phase along with a progressive lateral extension of movements. The area affected by movement appears in fact larger in the cumulated LOS displacement map from August 2nd 2015 to October 8th 2015 (Fig. 12). The analysis of the time series showed in Fig. 10c revels that the acceleration phase was ongoing during the execution of the second GBInSAR survey (October), especially from 10th October 2015.

2.5 GBInSAR versus in situ monitoring and implications for the landslide's kinematic

In Fig.s 13 and 14 the crack aperture measured by the E1, E2 and E3 extensometers is compared with the GBInSAR time series of the corresponding pixels in the maps obtained respectively through one of the weekly continuous surveys (October 2015) and through the discontinuous monitoring (July-October 2015). Data are also plotted along with the air temperature measured by the weather station installed on the landslide site (Fig. 2). The GBInSAR time series of Fig. 13 highlight LOS displacement within ±0.2 mm, thus indicating a general absence of movements for the respective points. The extensometers data show instead cyclic daily variations up to ±4 mm for the E2 instrument which appear to be strongly correlated to the short-term (i.e. daily) air temperature variations recorded on the site. A similar behaviour between the two datasets can be obtained by analyzing Fig. 14: the displacement retrieved through the GBInSAR monitoring is comprised between ±0.2 mm whereas the extensometers curves highlight cyclic variations up to ±7.0 mm, well correlated to the thermal air temperature changes. Due to the lack of the wire protection (Fig. 3), factors such as the snow accumulation at the base of the landslide scarp, the formation of ice on the cable and on the pulley and rocks detaching from the scarp and impacting on the device have been randomly disturbing the extensometric measures. The overall reliability of the extensometric measurements in this current setup therefore can be considered low.

Even though the two measurements techniques are not linked together, due to the different quantities measured (i.e. areal movements on surface versus point wise crack opening/closure), data shown in Fig.s 13 and 14 highlight that the GBInSAR technique is more effective and reliable than point-wise extensometers to monitor the superficial displacement of the Comba Citrin landslide.

The absence of apparent movement in the landslide crown sector and the main perimetral tension crack, as obtained from the GBInSAR discontinuous monitoring (Fig. 12), has furthermore

important potential implications for the kinematics of the landslide. Since the discontinuous GBInSAR surveys have identified a displacement between -2 and -5 mm from August to October 2015 in the landslide body, the absence of movements in the landslide crown sector implies a progressive down slope shift of the moving area which took place in the last few years. The development of further parallel cracks down slope to the main tension crack, a pattern which was already observed during the first phases of the landslide reactivation, could then explain this behaviour. This conclusion needs to be definitely confirmed by a specific geo-engineering survey of the area.

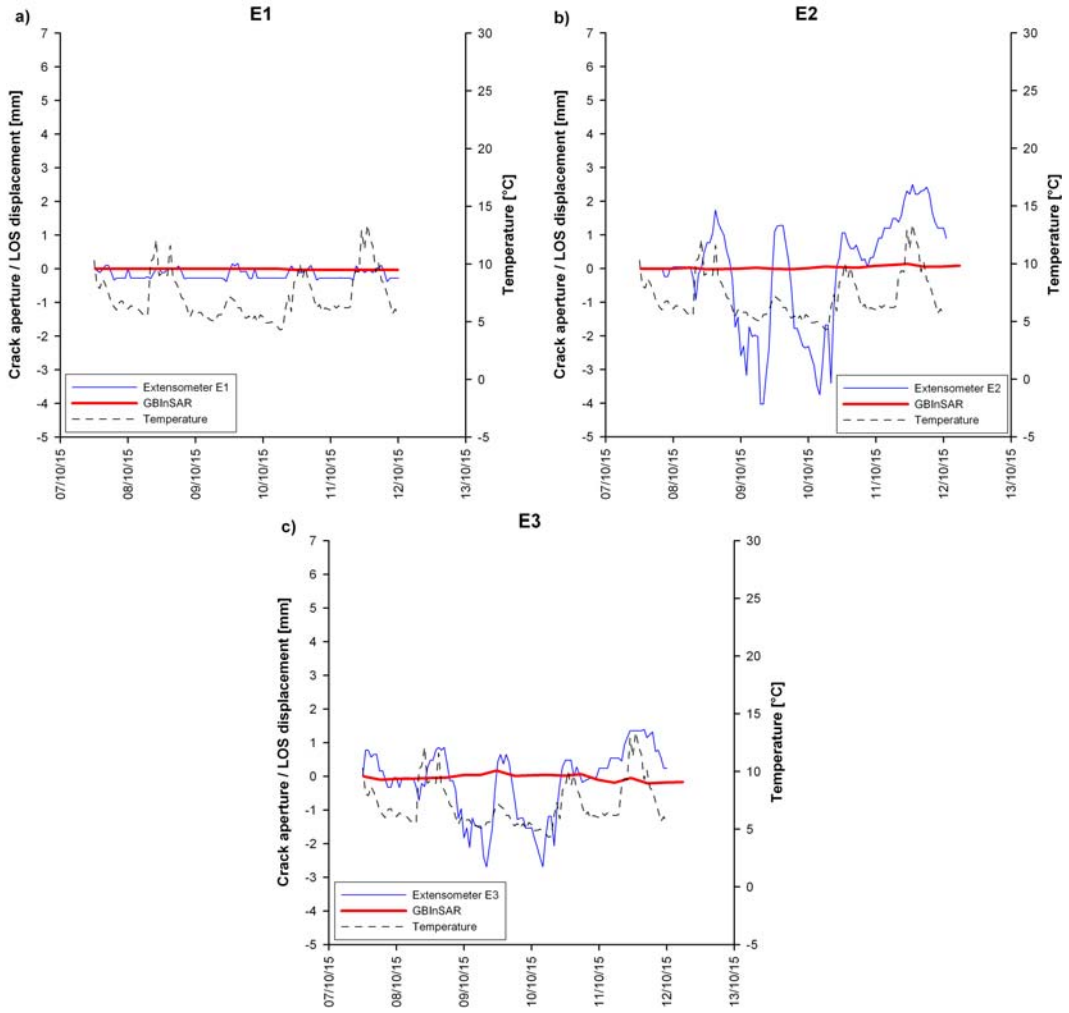

Fig. 13 – Comparison between GBInSAR LOS displacements measured during the October 2015 survey and crack aperture measured by extensometers E1 (a), E2 (b) and E3 (c). See Fig. 8 for location of the extensometers.

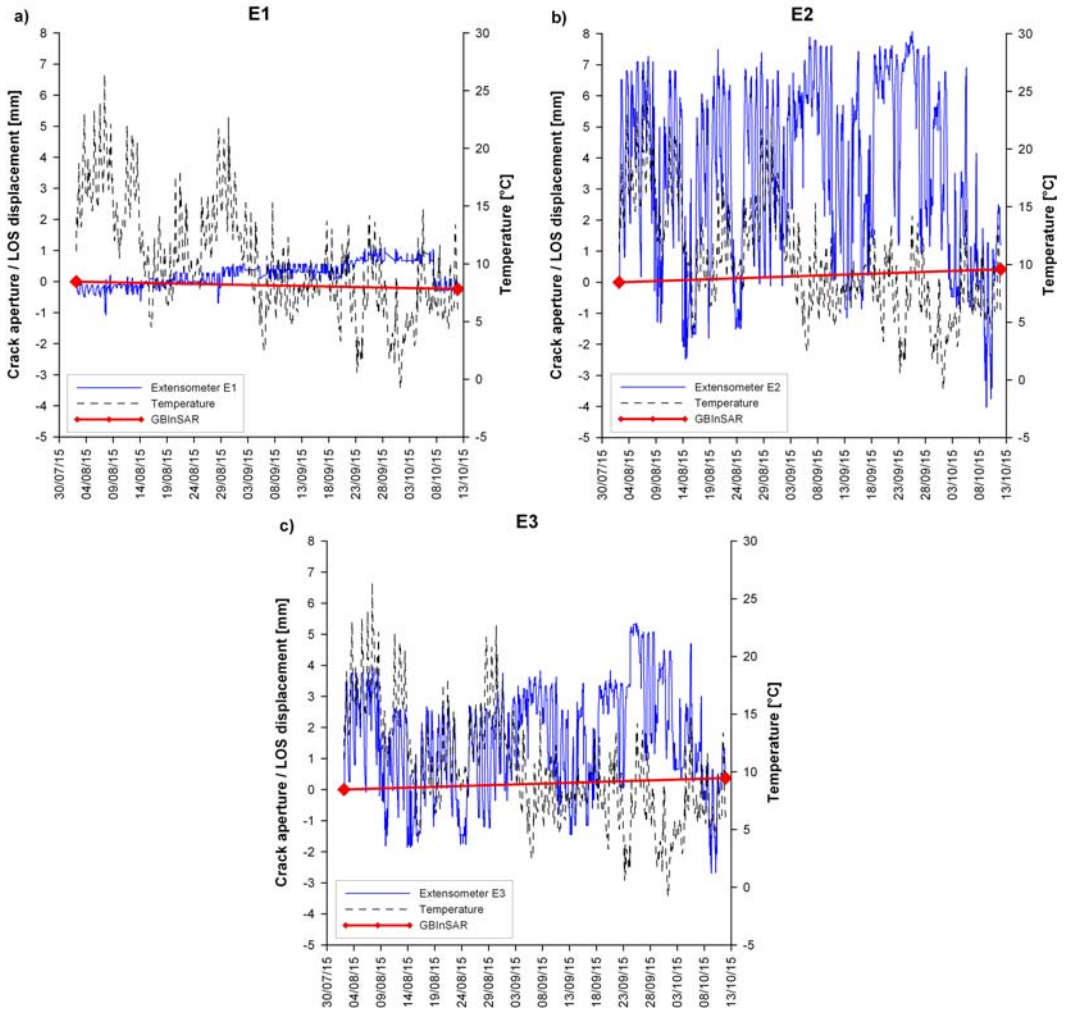

Fig. 14 – Comparison between GBInSAR LOS displacement measured from August 2nd 2015 to October 8th 2015 and crack aperture measured by extensometers E1 (a), E2 (b) and E3 (c). See Fig. 8 for location of the extensometers.

3. Discussion and conclusions

In this paper the results of two GBInSAR monitoring surveys of the Comba Citrin landslide and the adjoining areas were shown. The two surveys are separated by a temporal baseline of 63 days. For each of the two surveys a radar device working at Ku band was used. Particular attention was posed in radar repositioning to avoid the introduction of geometric baseline in subsequent measurement campaigns. The stack of SAR images of each survey were analyzed both separately and in combination to detect the possible displacements occurred both in every single survey by means of a

continuous processing as well as in the elapsed time between the two different campaigns by means of a discontinuous processing. For the discontinuous processing a set of different interferograms was obtained by cross-combining the SAR images of the different surveys. From the obtained coherence matrix, the best 40 interferograms characterized by the highest values of complex coherence were selected and used in the subsequent processing to retrieve the displacement occurred between the two surveys, after the estimation and the removal of atmospheric phase screen and the phase unwrapping procedure. The obtained results showed the presence of two different areas affected by millimetres to centimetres displacements on the monitored slope. In particular one moving sector outside the landslide boundaries was identified for the first time.

The adopted processing scheme allowed retrieving reliable displacement data on the whole monitored slope and to gain an insight on their spatial and temporal evolution during the intervening 2.5 months. Differently from previous discontinuous GBInSAR monitoring experiences, neither a priori information on the slope deformation velocities nor specific integrations with other monitoring techniques were used in this work to solve the phase ambiguity. The optimal separation time between consecutive discontinuous GBInSAR campaigns, i.e. the time to avoid or limit the aliasing effects on the interferograms, was instead directly assessed from the displacement obtained by means of the first survey (July-August 2015).

The outcomes of the discontinuous GBInSAR monitoring indicated that the technique was capable to measure with good precision, accuracy and spatial continuity the very slow displacement rate of the Comba Citrin landslide, which otherwise could have been monitored only through a continuous radar survey with an equivalent duration, a more demanding task both technically as well as economically. Moreover in this specific case the discontinuous GBInSAR has demonstrated to be more effective and reliable than point-wise in situ instruments to monitor landslide's superficial displacements.

More generally, the results obtained so far on the Comba Citrin landslide suggest the applicability of the discontinuous GBInSAR technique to monitor the very slow displacement of rock landslides, widespread in the Alpine region, where many good scatterers are present. By selecting these points from the SAR images even separated by large temporal baseline (e.g. weeks or months) it is hence possible to exploit the interferometric phase to retrieve the displacement pattern of the monitored slopes.

Acknowledgements

The authors would like to thank the Municipality of Saint Rhémy en Bosses and the Corpo Forestale dello Stato – Stazione di Étroubles (AO) for the help provided during the execution of the radar surveys.

References

Antolini F., 2014. The use of radar interferometry and finite-discrete modelling for the analysis of rock landslides. PhD Thesis, Politecnico di Torino, 272 pp.

Alba M., Bernardini G., Giussani A., Ricci P.P., Roncoroni F., Scaioni M., Valgoic P., Zhangd K., 2008. Measurements of dam deformation by terrestrial interferometric techniques. International Archives of Photogrammetry and Remote Sensing Spatial Information Sciences, 37 (part b1), 133-139.

Aresys, 2014. GRAPeS version 3.6 (Computer Software). Aresys, Milano, 2014.

Aresys, 2015. Repeat Pass version 01.01.012 (Computer Software). Aresys, Milano, 2015.

Atzeni C., Barla M., Pieraccini M., Antolini F., 2015. Early warning monitoring of natural and engineered slopes with Ground-Based Synthetic Aperture Radar. Rock Mechanics and Rock Engineering, 48, 235–246.

Barla G., Antolini F., Barla M., Mensi E., Piovano G., 2010. Monitoring of the Beauregard landslide (Aosta Valley, Italy) using advanced and conventional techniques. Engineering Geology, 116, 218-235.

Barla M., Antolini F., 2015a. Monitoring geotechnical structures by ground based radar interferometry. 7th International Conference on Structural Health Monitoring of Intelligent Infrastructures SHMII (SHMII-7 2015), Torino 1-3 July 2015, 10 pp.

Barla M., Antolini F., 2015b. An integrated methodology for landslides' early warning systems. Landslides, DOI: 10.1007/s10346-015-0563-8.

Berardino P., Fornaro G., Lanari R., 2002. A new algorithm for Surface Deformation Monitoring Based on Small BaselineDifferential SAR Interferograms. IEEE Transactions on Geoscience and Remote Sensing, 40 (11), 2375-2383.

Casagli N., Catani F., Del Ventisette C., Luzi G., 2010. Monitoring, prediction, and early warning

using ground-based radar interferometry. Landslides 7(3), 291–301.

Corsini A., Ciccarese G., Ronchetti F., Bertacchini E., Berti M., Truffelli G., Generali M., Pizziolo M., Gallucci A., Gozza G., Monni A., Pancioli V., 2011. Testing the applicability of ground-based interferometric SAR in several "typical" landslides of Emilia Romagna Apennines with a civil protection perspective. The II World Landslides Forum Abstract – WLF2, Rome 3-9 October 2011, 2011-0528, 207.

Crosetto M., Monserrat O., Luzi G., Cuevas-González M., Devanthéry N., 2014. Discontinuous GBSAR deformation monitoring. Journal of Photogrammetry and Remote Sensing, 93, 136-141.

Cruden D.M., Varnes D.J. 1996. Chapter 3 - Landslide types and processes. In A.K. Turner, R.L. Schuster (Eds.), Landslides Investigation and Mitigation. Special Report 247, Transportation Research Board, National Research Council, National Academy Press, Washington, DC (1996), 36–75.

Farina P., Coli N., Yön R., Eken G., Ketizmen H., 2013. Efficient real time stability monitoring of mine walls: the çöllocar mine case study. In: Proc. International Mining Congress and Exhibition of Turkey, Antalya (Turkey), 16-19 April 2013, 111-117.

Ferretti A., Prati C., Rocca F., 2001. Permanent scatterers in SAR interferometry. IEEE Transactions on Geosciences and Remote Sensing, 39(1), 8-20.

Hydrodata 2005. Risques hydro-géologiques en montagne: parades et surveillance - RiskHydrogeo – L'eboulement de masse de Citrin: description du site de visite. Electronic file.

Intrieri E., Di Traglia F., Del Ventisette C., Gigli G., Mugnai F., Luzi G., Casagli N., 2013. Flank instability of Stromboli volcano (Aeolian Islands, Southern Italy): integration of GB-InSAR and geomorphological observations. Geomorphology 201, 60-69.

Luzi G., Monserrat O., Crosetto M., Copons R., Altimir J., 2010. Ground-Based SAR interferometry applied to landslide monitoring in mountainous areas. Proceedings of Mountain Risks conference: Bringing science to society, Florence (Italy), 24-26 November 2010.

Mariotti F., Amoroso G., Giudici D., D'Aria D., Farina P., 2012. Slope monitoring within open-pit mines by ground-based radar: methodology, data processing and case studies review. In: Proceedings of the symposium on the application of geophysics to engineering and environmental problems (SAGEEP 2012), Tucson, 25–29 March 2012.

Monserrat O., Crosetto M., Luzi G., 2014. A review of ground-based SAR interferometry for deformation measurement. Journal of Photogrammetry and Remote Sensing, 93, 40-48.

Noferini L., Pieraccini M., Mecatti D., Luzi G., Tamburini A., Broccolato M., Atzeni C., 2005a. Permanent scatterers analysis for atmospheric correction in Ground-Based SAR interferometry. IEEE Transactions on Geosciences and Remote Sensing, 43(7), 1459–1471.

Noferini L., Pieraccini M., Mecatti D., Macaluso G., Luzi G., Atzeni C., 2005b. Long term landslide monitoring by ground-based synthetic aperture radar interferometer. International Journal of Remote Sensing, 27(10), 1893-1905.

Noferini L., Takayama T., Pieraccini M., Mecatti D., Macaluso G., Luzi G., Atzeni C., 2008. Analysis of Ground-Based SAR data with diverse temporal baseline. IEEE Transaction on Geoscience and Remote Sensing, 46(6), 1614-1623.

Ratto S., Bonetto F., Comoglio F., 2003. The October 200° flooding in Valle d'Aosta (Italy): Event description and land planning measures for the risk mitigation. International Journal of River Basin Management, 1:2, 105-116.

Rudolf H., Leva D., Tarchi D., Sieber A.J., 1999. A mobile and versatile SAR system. Proceedings of International Geoscience and Remote Sensing Symposium, (IGARSS 1999), 592–594, Hamburg (Germany), IEEE 1999 International.

Strozzi T., Werner C., Wiesmann A., Wegmuller U., 2012. Topography mapping with a portable real-aperture radar interferometer. IEEE Geoscience and Remote Sensing Letter, 9(2), 277-281.

Tapete D., Casagli N., Luzi G., Fanti R., Gigli G., Leva D., 2013. Integrating radar and laser-based remote sensing techniques for monitoring structural deformation of archaeological monuments. Journal of Archaeological Sciences, 40(1), 176-189.

Tarchi D., Casagli N., Fanti R., Leva D., Luzi G., Pasuto A., Pieraccini M., Silvano S., 2003. Landslide monitoring by using ground-based SAR interferometry: an example of application to the Tessina landslide in Italy. Engineering Geology, 68(1–2), 15–30.

Wasowski J., and F. Bovenga, 2014a. Investigating landslides and unstable slopes with satellite Multi Temporal Interferometry: Current issues and future perspectives. Engineering Geology, 174, 103–138.

Wasowski J., and F. Bovenga, 2014b. Remote Sensing of Landslide Motion with Emphasis on Satellite Multitemporal Interferometry. In: T. Davis and J. Shroder (eds.), Landslide Hazards, Risks, and Disasters, Chapter 11, 345-403, Elsevier. http://dx.doi.org/10.1016/B978-0-12-396452-6.00011-2

Wujanz D., Neitzel F., Hebel H.P., Linke J., Busch W., 2013. Terrestrial radar and laser scanning for deformation monitoring: first steps towards assisted radar scanning. ISPRS Annals, Vol. II-5/W2, ISPRS Workshop Laser ScannING 2013, 11-13 November 2013 Antalya, Turkey.